Study of low-frequency quasi-periodic oscillations in GRS 1739–278 during 2014 outburst

Authors[1]

[1]*Space Research Institute, Russian Academy of Sciences, Profsoyuznaya 84/32, 117997 Moscow, Russia*

ABSTRACT

Key words: X-rays: individual (GRS 1739–278) – accretion, accretion disks

We detected low-frequency quasi-periodic oscillations (QPOs) at 0.3..2 Hz in *NuSTAR* and *Swift-XRT* observations of black hole candidate GRS 1739–278 during its 2014 outburst.

1 INTRODUCTION

A study of X-ray variability in accreting astrophysical sources provides a broad view on processes that take a place in such systems. This works both on a long timescales - i.e. days and weeks - when one speak about state changes through outbursts of transients sources (see e.g. Homan and Belloni 2005a; Heil et al. 2015), and on short - all the way down to milliseconds - when the subject under consideration are a quasi-periodic oscillations (QPOs). By simultaneous usage of spectral and timing data one can better constrain geometry of accretion flow around compact objects and infer on which processes are responsible for generation of observed spectro-timing features in a self-consistent way.

Some aspects of the spectro-timing evolution of the X-ray transients (usually black-hole candidates, BHC) during outbursts can be explained in the frame of the two-temperature accretion flow model (Eardley et al. 1975; Shapiro et al. 1976; Narayan and Yi 1995), in which geometry of system consists of the geometrically thin cold disk and geometrically thick hot flow (corona), which is thought to be responsible for production of strong variability. As example, using frequency-resolved spectroscopy Churazov et al. (2001) shown that variable part of the emission has a hard spectrum, produced by Comptonization of soft photons onto hot electrons in the corona, while stable part of the emission has a spectrum which is consistent with the cold classical α-disc spectrum (Shakura and Sunyaev 1973). Lyubarskii (1997) proposed that observed strong variability (seen as a broad band noise in power spectra) is produced due to the stochastic variations of the angular momentum transport efficiency. In this propagating fluctuation model broad band noise is a product of noise signals from different radii of the accretion flow, each with its own characteristic time-scale (see, e.g. Arévalo and Uttley 2006; Ingram and van der Klis 2013). Therefore, the shape of the broad band noise is determined by the physical and geometrical properties of the accretion flow, e.g. in particular in these works it was sug-

gested that the broad noise dumping frequency is connected to the inner edge of the accretion flow.

Another feature, frequently observed in the X-ray binaries power spectra is different types of low and high frequency QPOs, manifesting itself as a narrow Lorentzian components. One of the long-standing questions in X-ray timing is the origin of so called type-C low-frequency QPOs (see Casella et al. 2005, for LFQPO classification), which are often found in X-ray binaries harboring both neutron stars and black-holes (Wijnands and van der Klis 1999a) during initial rise and transition to disk dominated state (in low-hard state (LHS) and in hard intermediate state (HIMS)), according to standard scheme (Grebenev et al. 1997; Tanaka and Shibazaki 1996; Remillard and McClintock 2006; Belloni 2010)). This QPOs are widespread and easy to detect and study, since they occur at moderate frequencies of 0.1..10 Hz and prominent, having $rms \approx 10\%$. Different author prescribe generation of this QPOs to various processes: Lense-Thirring precession of inner parts of accretion disk (Stella and Vietri 1998a; Ingram et al. 2009a), oscillations of standing shock (Molteni et al. 1996), accretion rate modulation caused by different phenomena (Tagger and Pellat 1999; Cabanac et al. 2010) e.t.c. In some models, particularly in relativistic precession models (RPM), observed frequency is strongly dependent on location of inner part of cold accretion disk.

Recent advances in simulating the reflection (Ross and Fabian 2005; **García** et al. 2014), arising from reproduction of emission from central engine by accretion disk, led to the possibility to study geometry of accretion disk in bright systems. For such a study to be made it is essential to obtain broadband X-ray spectrum with high energy resolution - reflected component manifest itself by a presence of prominent, wide and asymmetric iron K_α-line at 6.4 keV and Compton-hump at 20-30 keV. Now, adding information from X-ray timing one can, in principle, constrain the location of a component, responsible for the variability - which is though to be corona or jet foundation. This task present a challenge, that can be solved only by a telescope

that posses both possibility to measure broadband spectrum with good resolution and have a corresponding timing capabilities. *NuSTAR* (Harrison et al. 2013), launched in 2013, is the best available instrument for such studies, although, except for observations in energy band above 12 keV, *XMM-Newton* (and *NICER* in the nearest future) can be used too, producing some great results (Ingram et al. 2016).

In this article we report on first detection of this QPOs in HIMS of Galactic black-hole candidate GRS 1739–278 and present a detailed study of properties of the X-ray variability, along with spectral evolution.

2   GRS 1739-278

GRS 1739–278 is a typical X-ray nova, discovered during outburst in 1996 (Paul et al. 1996) by *SIGMA* (Paul et al. 1991) telescope onboard *GRANAT* space observatory. Using *ROSAT* observation Greiner et al. (1996) inferred distance of 6–8.5 kpc, indicating that source may belong to Galactic bulge. Optical and radio emission were detected during the course of outburst (Hjellming et al. 1996; Marti et al. 1997). Borozdin et al. (1998) found spectral evolution throughout outburst to be consistent with canonical model - outburst starts from LHC, then soft component, associated with disk emission starts to dominate, heralding transition to high-soft state. Eventually, they observed very high state and detected a QPO at 5 Hz using *RXTE* data (Borozdin and Trudolyubov 2000).

After some 18 year slumber GRS 1739–278 demonstrated another big outburst, rise of which was detected by *Swift-BAT* (Krimm et al. 2014) along with *INTEGRAL* (Filippova et al. 2014). During this outburst extensive observing campaign by *Swift-XRT* were carried out, along with single long *NuSTAR* exposure. We will utilize this data in following chapters. After this outburst source remain active with repetitive mini-outbursts (Mereminskiy et al. 2016; Yan and Yu 2017).

3   OBSERVATIONS AND DATA REDUCTION

In order to characterize the overall outburst profile we used data of *Swift-BAT* transient monitor (Krimm et al. 2013) in hard X-rays (15–50 keV) as well as data from *MAXI* (Matsuoka et al. 2009) (2–4 keV).

We used public observations of *Swift-XRT* (target ID: 33203) performed regular over the peak and decline of the outburst. Since the source was bright, all *Swift-XRT* observations were performed in windowed mode, allowing study of timing properties of the source. We performed standard analysis with `xrtpipeline` and barycentered data prior to lightcurve extraction. During several observations countrate was as high as 280 cts s^{-1}, therefore we excluded one or few brightest columns, in order to suppress effects caused by photon pile-up. Photons with energies below 0.8 keV and above 10 keV were also filtered out. Long-term lightcurves and spectra were obtained from UK Swift Science Data Centre at the University of Leicester (Evans et al. 2009).

We also used *NuSTAR* observation (ObsID: 80002018002) performed at March 26, 2014 (MJD 56742). `nuproducts` pipeline were utilized to extract photons from two-arcminute circular region, centered on source and to produce lightcurves and spectra.

4   ANALYSIS

4.1   Outburst

First detection of the source by *Swift-BAT* (Krimm et al. 2014) occurred at March 9, 2014 (MJD 56725, we will refer to this date as τ_0). Outburst profile in hard X-rays (15–50 keV) featured fast rise with tenfold intensity increase over ten days, nearly flat-top peak ($\tau_0+10..+15$) followed by abrupt flux decrease by 30% over two days. After this, source demonstrated gradual decline interrupted by flaring activity at $\tau_0+30..+65$. Another interesting feature is dip, observed in *Swift-BAT* lightcurve at $\tau_0 \approx +86$. After the cease of the outburst source remained active with flux about 5–15 mCrab.

Adding softer data from *MAXI* to the *Swift-BAT* hard X-ray lightcurve gives us another insight on evolution of the outburst as shown in Fig. 1 - comparing fluxes in soft and hard bands (for 2–4 keV band we took a 1.67 counts s^{-1} as a reference value for Crab, corresponding value for 15–50 keV band is 0.22 cts cm^{-2} s^{-1}) one can see that soft component obviously lags hard emission in the beginning of the outburst but then start to grow and ends up dominating during the flaring period as well as hard dip(s). Lower subplot of Fig. 1 shows evolution of hardness ratio (3–10 keV/0.8–3 keV) measured by *Swift-XRT*. Right after peak of hard X-rays one can see decline of hardness, also indicating appearance of thermal component.

Fortunately, the *NuSTAR* observation triggered by Miller et al. (2015) were carried right at the transition between hard and soft states, thus giving us unique possibility to study processes that happens during HIMS.

4.2   NuSTAR observation

NuSTAR observed GRS 1739–278 (ObsID: 80002018002) for nearly 30 ks of dead-time corrected exposure right after hard X-ray peak (see Fig. 1). Earlier, Miller et al. (2015) shown that the average spectrum of this observation is well described by reflection models such as *relxill* (**García** et al. 2014; Dauser et al. 2014, 2016) with accretion disk that reaches remarkably close to the black hole innermost stable circular orbit (ISCO), with upper estimate being $r_{in} = 5^{+3}_{-4} \, GM/c^2$ (Miller et al. 2015). Interestingly, no additional thermal component was needed in order to obtain a good fit, probably because of *NuSTAR* energy band, starting at 3 keV.

Given the 96.9 minute orbital period of *NuSTAR*, observation is divided in 13 intervals separated by Earth occultations, as shown in Fig. 2. We denoted this intervals with roman numerals, from **I** to **XIII**. From the lightcurve of observation it is clear, that source flux is increasing throughout observation from $\approx$145 counts per second up to $\approx$170 counts per second. The spectrum also alter, with hardness (defined as ratio of countrates $R_{3-10 \, keV}/R_{10-78 \, keV}$) monotonically growing from 2.5 to 3.5.
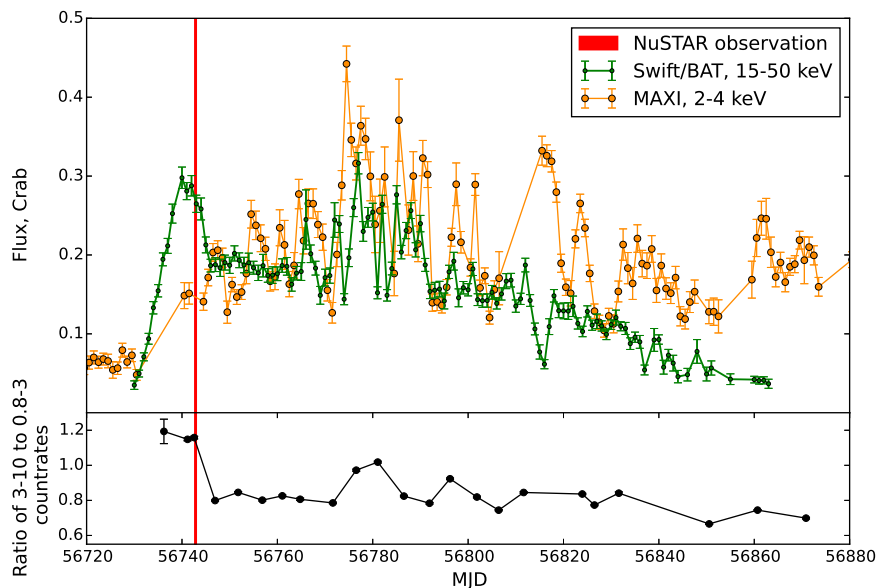
Figure 1. *Upper:* green points denote *Swift-BAT* lightcurve of second outburst in 15–50 keV range, orange circles correspond to *MAXI* fluxes in 2–4 keV. Red line show time of *NuSTAR* observation. *Lower:* evolution of *Swift-XRT* spectral hardness during the outburst.

4.2.1 Continuum evolution

To get better view on evolution of continuum emission we fitted using `XSPEC` package (Arnaud 1996) all individual interval spectra with `xillver` model (García et al. 2013). This model describes reflection of incident radiation from ionized slab of matter. The spectrum of incident radiation are assumed to be power-law with exponential cutoff. Spectra from two *NuSTAR* modules of each interval were fitted simultaneously with `phabs*const*xillver` model. We choose to fix interstellar absorption at $N_H = 2.15 \times 10^{22}$ cm^{-2} as was found by joint *XMM-Newton/NuSTAR* observation during low luminosity state (Fuerst et al. 2016). Element abundances were taken from Wilms et al. (2000) and cross-sections from Verner et al. (1996). Relative iron abundance were fixed at $A_{Fe} = 1$, ionization parameter at $\xi = 3.2$ and inclination at 35 degrees. This parameters are in agreement with measured by Miller et al. (2015) with different spectral models. Although in `xillver` there is no relativistic broadening of Fe-line no significant residuals in 5–8 keV region are seen, mainly because of limited statistics in per interval spectra. Before fitting, spectra were grouped in order to have at least 100 counts per bin, channels above 60 keV were ignored. Resulting fits are of satisfactory quality with mean $\chi^2_{red.} \approx 1.05$.

Examination of best-fit parameters shown in Fig.4 confirms that spectrum softens during observation and cutoff energy decreases. Flux is steadily increasing and at the end of observation unabsorbed luminosity in 3–60 keV band reach 7×10^{37} erg s^{-1} assuming 8 kpc distance.

4.2.2 Constrains on movement of the inner parts of accretion disk

Yet, spectra of single intervals have not enough statistics to constrain change of Fe-line profile and, hence, to determine

is the inner boundary of disk is moving during observation. To increase statistics, we split whole observation into three major pieces, with first made by intervals **I-IV**, second by **V-IX** and third by **X-XIII** and extracted 4–78 keV spectra. We chose to group them in order to have at least 100 counts per bin and then we fitted them (excluding data between 5–10 keV) with simple `phabs*cutoffpl` model, using, once again, $N_H = 2.15 \times 10^{22}$ cm^{-2}.

Now, plotting the ratio of this fit to initial spectra (see Fig. 3) one can see that both strong features - i.e. Fe-line complex at 5–9 keV and Compton hump around 30 keV are seemingly stable. Therefore we can conclude, that there is no drastic change in position of inner disk boundary between parts of observation. Additionally, we estimated equivalent width of Fe-line in this three parts - we approximated 4–78 keV spectra with 10–30 keV range being ignored (to neglect the Compton-hump contribution) with model consisting of absorbed cut-off powerlaw and gaussian. Equivalent width of gaussian component remain constant within error margins, around 0.175 keV, although it is possible that the quality of data is not enough to trace the real change.

4.2.3 Characterization of the average spectrum

There is a 1.3 ks part of *Swift-XRT* snapshot (ObsId: 00033203003) that coincides with *NuSTAR* observation. Extension of an energy range to 0.8 to 78 keV allow one to search for thermal emission associated with cold inner disk with $kT \sim 0.1...0.4$ keV (such as were found in other BHCs, see (Miller et al. 2006a,b; Parker et al. 2015, e.t.c)).

We extracted *Swift-XRT* spectrum using only zero-grade events, and grouped it (as well as *NuSTAR* spectra) to have at least 30 counts per bin and added 3% systematic error. We used latest available version of *relxilllp* package (v1.0.2), the model that describes reflection of emission produced by point source located on the rotation axis above the
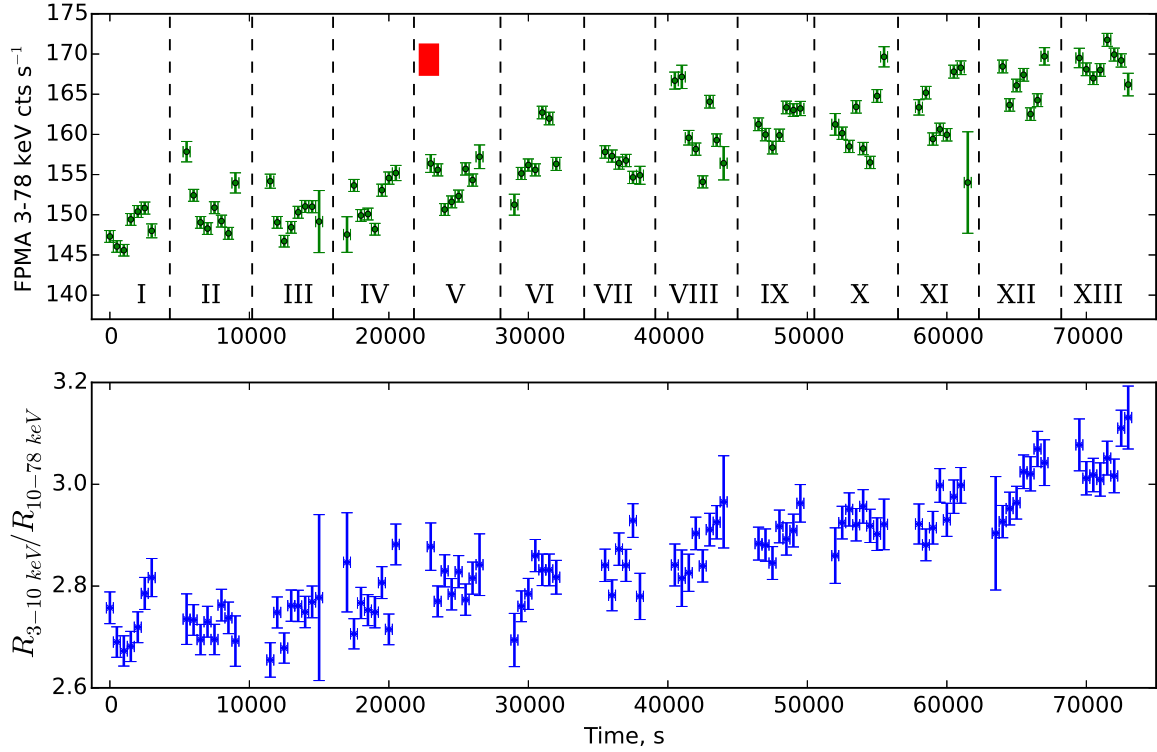
Figure 2. Upper panel: countrate of *NuSTAR* FPMA in 3–78 keV band. We enumerated intervals of uninterrupted observations with roman numerals. Red square shows time of simultaneous *Swift-XRT* observation (ObsId: 00033203003, second part). Bottom panel: evolution of hardness during observation
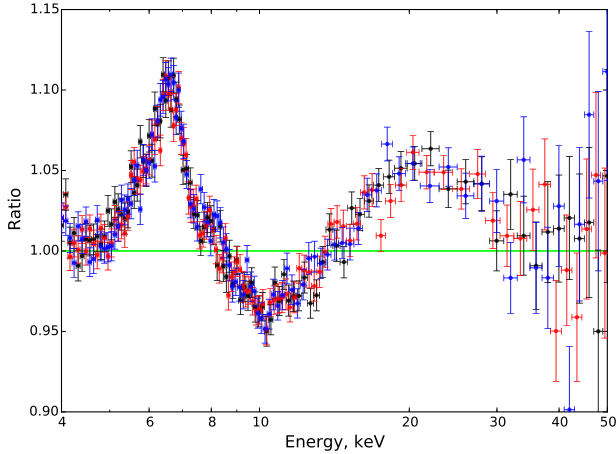

Figure 3. Ratio of *NuSTAR* FMPA, spectra to `phabs*cutoffpl` model. In black - data from intervals I-IV, in red from V-IX and in blue from X-XIII.

Kerr black hole from the relativistic accretion disk. Among the parameters of a model several of a particular interest namely h - height of point source above the black hole and R_{in}, location of the inner boundary of accretion disk. This model was selected for several reasons - first, Miller et al. (2015) found that it match observed data well producing least strigthent constraints on inner radius of the disk. Also,

during the 1996 outburst source was detected at radiowaves, possibly indicating jet activity.

Interestingly, instead of surplus thermal component we found a lack of soft emission - usage of $N_H = 2.15 \times 10^{22}$ cm^{-2}, measured in source low state (**?**) led to worse fits with systematic negative residuals below few keV. Therefore, we left N_H free during the fit. Obtained value of 2.6×10^{22} cm^{-2} is higher than one measured by **?**. This can be possibly accounted to presence of disk outflow, caused by severe X-ray irradiation.

Other parameter values match well with measurements by Miller et al. (2015).

5   TIMING ANALYSIS

Variability properties of different types of X-ray binary systems are usually described in terms of the power spectrum, which is a common technique for determination of amount of power in the particular frequency range. Power spectrum of the BHC systems in LHS typically can be described as a combination of band-limited noise and one or few narrow Lorentzian functions, representing correspondingly broad band stochastic noise and QPOs (see, e.g. Terrell 1972; Belloni and Hasinger 1990; Homan and Belloni 2005b, e.t.c). Properties of this components and correlations between them, in principle, may be used to discriminate between different models, proposed for generation of X-ray emission in BHC.
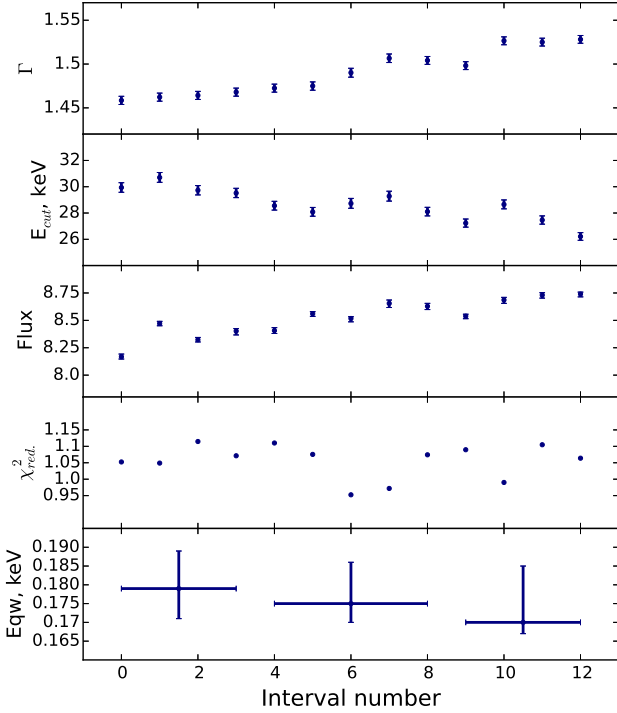
Figure 4. Parameters of continuum emission in intervals. From upper to lower: `xillver` powerlaw slope, cutoff energy, flux in 3–60 keV band $\times$ erg s^{-1} cm^{-2}, χ^2 per degree of freedom and Fe-line equivalent width.

Figure 5. Estimate of inner radius of accretion disk. Gray solid line denote 90% confidence interval, while dashed line shows 99% interval.

Table 1. Best-fit parameters of `phabs*relxilllp` model

Parameter	Value
N_H	$2.65^{+0.04}_{-0.02}$
h	$19.2^{+2.8}_{-2.2}$
a	$0.76^{+0.21}_{-0.47}$
$incl$	$24.3^{+1.7}_{-2.4}$
R_{in}	1.25000
Γ	$1.40^{+0.01}_{-0.01}$
$\log \xi$	$3.48^{+0.04}_{-0.03}$
A_{Fe}	$3.0^{+0.3}_{-0.2}$
E_{cut}	$26.2^{+0.4}_{-0.3}$
R_{refl}	$0.44^{+0.03}_{-0.04}$
$N, \times 10^{-2}$	$1.54^{+0.07}_{-0.06}$
C_{FMPB}	$1.018^{+0.001}_{-0.001}$
$C_{Swift-XRT}$	$1.04^{+0.001}_{-0.001}$
$\chi^2_{red.}$	$1.1=$
	$= 3366.81/3075$ d.o.f

Although power spectra analysis is by far the most popular, more sophisticated methods, such as coherence function or phase-lag were successfully used to infer physical properties of accretion flows. Using a measured time-lag between the soft and hard emission, which have a complex behavior with the frequency, Nowak et al. (1999) constrained geometrical size of the accretion flow.

In the following section we present analysis of the timing properties and their evolution during the 2014 outburst of GRS 1739–278 .
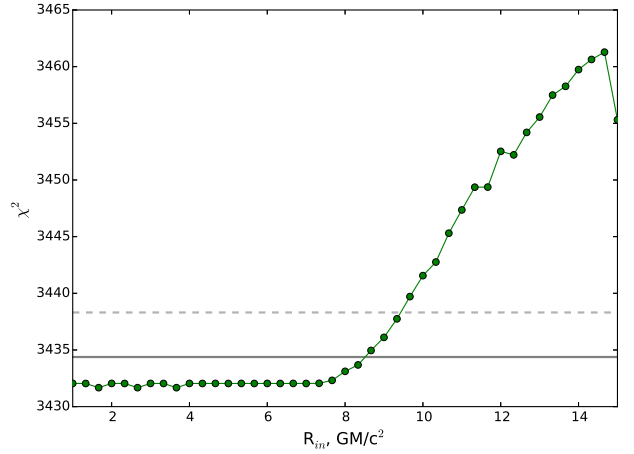
5.1 Power spectrum

NuSTAR observation of the GRS 1739–278 2014 outburst are split on 13 continuous parts separated with ~ 0.7 hr intervals when the source was occulted by Earth. The continuous observations have duration from ~ 2440 to ~ 3390 sec see Table **??**. Since *NuSTAR* detectors operate in the photons counting mode, data can be reduced to the light-curve with time resolution up to 2μs. For our analysis we extracted light-curves with 0.01 s temporal resolution, therefore we obtained power spectra in the $sim 3 \times 10^{-3}$–50 Hz range. This is a frequency range which usually contains low frequency quasi periodic oscillations QPOs and broad band noise component (Wijnands and van der Klis 1999b). We didn't try to found high frequency QPOs, since the typical HF QPO (centroid frequency 100-400 Hz, amplitude $\approx 10\%$ and quality $Q \approx 0.1$–0.5) is indiscernible over the Poisson noise with the obtained count-rate.

The power spectrum of each of the separate observations has a form of a white noise plateau ($P(f) \propto const$) on the low frequencies, transforming on the frequency ≈ 0.1 Hz in to the power law with the slope $\rho \approx -1.6$––2.0. Also a prominent QPO on the frequencies 0.3–0.7 Hz and its second overtone is presented. Typical power spectrum of single interval is shown in Fig. 6. Poisson noise dominates intrinsic source variability on the frequencies over ≈ 2 Hz, preventing analysis of any high-frequency features. There is also signs that the Power spectrum on the frequencies below ≈ 0.003 Hz has a form of growing power law $P(f) \propto f^\alpha$, $\alpha > 0$.

From the shape of the energy and Fourier spectrum we concluded that the system is in the hard intermediate state and observed low frequency QPO (LF QPO) is of type C.

In order to assess properties of the variability power spectra we approximate each obtained power spectra with

the following analytical function:

$$P(f) = n(1 + (f/f_{\text{lb}})^4)^\alpha +$$
$$\frac{s_1}{(f - f_{qpo})^2 + (f_{\text{qpo}}Q_{\text{m}})^2} +$$
$$\frac{s_2}{(f - 2f_{qpo})^2 + (2f_{\text{qpo}}Q_{\text{m}})^2} +$$
$$+ poiss \qquad (1)$$

In this function first component represents plateau with the break, second two components describe QPO main harmonics and its overtone, last component represents constant Poisson noise.

Due to the complex dead-time behaviour over the energy, it's impact on to the power spectrum can not be well described. This method is based on the following assumption: since photons arrival times are independent for the two detectors, phases of the Fourier function of two light-curves are also random and independent. It follows that this cross-product is a complex value with random uniformly distributed phase and the mean of it's real part is zero. Following Bachetti et al. (2015) we calling obtained function cross-spectrum or cospectrum.

While cross-spectrum technique works perfectly for the power spectrum assessment, we still using classical Fourier power spectrum for the analysis in this work due to the following reason. Each value of the cross-spectrum belongs to the distribution with a complex probability density function (PDF), which, for the random independent signals in two detectors, can be described with the special Bessel function of second kind and has a different PDF for a coherent signals. Since this distribution has finite standard deviation, according to the central limit theorem, distribution of the sum of the values tends toward a normal distribution. To track the source variability evolution we fitting relatively short observations with duration of 2–3 ks, and therefore can not split them more than to few dozens parts in order to have an eye on the power spectrum break feature on the 0.1 Hz frequency. We found that usual root mean square technique, used to fit normally distributed values, works not stable in that case, probably because the PDF is not yet close enough to the normal distribution.

To simplify our analysis we inspect power spectrum only on frequencies above 10 Hz, allowing Poisson noise to has arbitrary power but assuming that it's power spectrum component is still flat $(P(f) = const)$.

We found that the QPO frequency and amplitude had clearly evolved with time see Table ?? and Figure 6. The QPO frequency correlates with the *NuSTAR* flux and photon index, similar to many other black hole and neutron star binary systems (see, e.g., Vignarca et al. 2003a; Pottschmidt et al. 2003). On the other hand we see, that the QPO amplitude was stable during the first half of the observation, and started to grow in the second part.

Some models suggest, that the type-C QPO arising due to the Lense-Thirring precession of the accretion flow inner parts (Stella and Vietri 1998b; Schnittman et al. 2006; Ingram et al. 2009b), in such models growth of the QPO frequency corresponds to the shrinking of the disk inner radius. However, sophisticated spectral models applied to the observed *NuSTAR* spectrum suggest that the accretion disk inner radius is $R_{\text{in}} = 5^{+3}_{-3}R_{\text{g}}$. This estimation is primarily based on the profile of the relativistically widened neutral

Iron fluorescent line, see section ?? and also (Miller et al. 2015).

We found that the QPO amplitude is smaller in the soft band, while amplitude of it's harmonic is bigger, the ratio of the power in the QPO and it's harmonic is 0.2 ± 0.1 in 10–78 keV band and 0.4 ± 0.1 in 3-5 energy band. It follows that the QPO profile, if it's presented (see, e.g. Ingram and van der Klis 2015), differs in the hard and soft X-ray band. Following (Ingram and van der Klis 2015) we tried to extract QPO profile segregating the coherent part between the QPO and it's harmonic, however no significant coherence was presented above the noise level, one can conclude that the QPO profile was not stable along the observation.

In some observation segments QPO subharmonics, centered approximately at the 1/2 of the QPO centroid frequency, is clearly observed in the cross-spectra (see examples on Figure ??, red crosses) (namely I, II, IV, V, VI sets). In order to observe QPO profile with better significance we summarized several cospectra, frequency of each cospectrum was scaled in such a way to conserve QPO centroid at 0.3 Hz. Obtained "tracked" cospectrum is presented on Figure 7. The subharmonics seems to roam around the 1/2 QPO frequency, therefore we were not able to obtain it with a large significance on the tracked spectrum.

It should be noted that the changes in the QPO centroid position during the interval may contribute to the observed quality factor Q. We can estimate the derivative of the QPO centroid position with time (by approximating $f_{\text{QPO}}(time)$ with the straight line), which appears to be $\dot{f}_{\text{QPO}} \approx 6.5 \times 10^{-6}$ Hz s^{-1}. During an interval with the duration $\tau = 3000$ s observed QPO drift will broaden the perfect QPO located at $f_{\text{QPO}} = 0.3$ Hz up to the quality factor $Q \approx \dot{f}_{\text{QPO}}\tau/f_{\text{QPO}} \approx 0.065$, which is of order of the Q estimations obtained from the observations with 1 model. In order to better estimate of the QPO quality factor, we split each of the 13 intervals in a set of 82 s time-series. We fitted power spectrum of all time-series simultaneously, substituting in the model 1 the QPO centroid frequency f_{qpo}, stimated for the model 1, with shifted frequency $f'_{\text{qpo}} = f_{\text{qpo}} + (t - t_{\text{mid}})\dot{f}_{\text{qpo}}$, with $\dot{f}_{\text{qpo}}$ being the free parameter and t_{mid} middle of the data set observation time interval. Inside each data set we obtained the QPO centroid changing speed consistent with the estimation obtained from the general trend, nevertheless the median quality factor, obtained in this model appears to be $\sim 7 \times 10^{-2}$ - i.e. compatible with the previous estimations (see Table 2). It should be noted that the estimation of the QPO quality factor is restricted with the width of fast Fourier transform frequency bins, which is 1/T, where T - is a duration of separate signals used for fitting, in our case $T = 82$ s, and QPO width is limited at $1/T = 0.012$ Hz.

In Table ?? one can find obtained fit parameters for the 13 *NuSTAR* intervals.

5.2 Coherence

(Vaughan and Nowak 1997) suggested to use coherence between different energy bands in order to obtain additional information from the source variability. Coherence measure the similarity between two signals and can be computed with
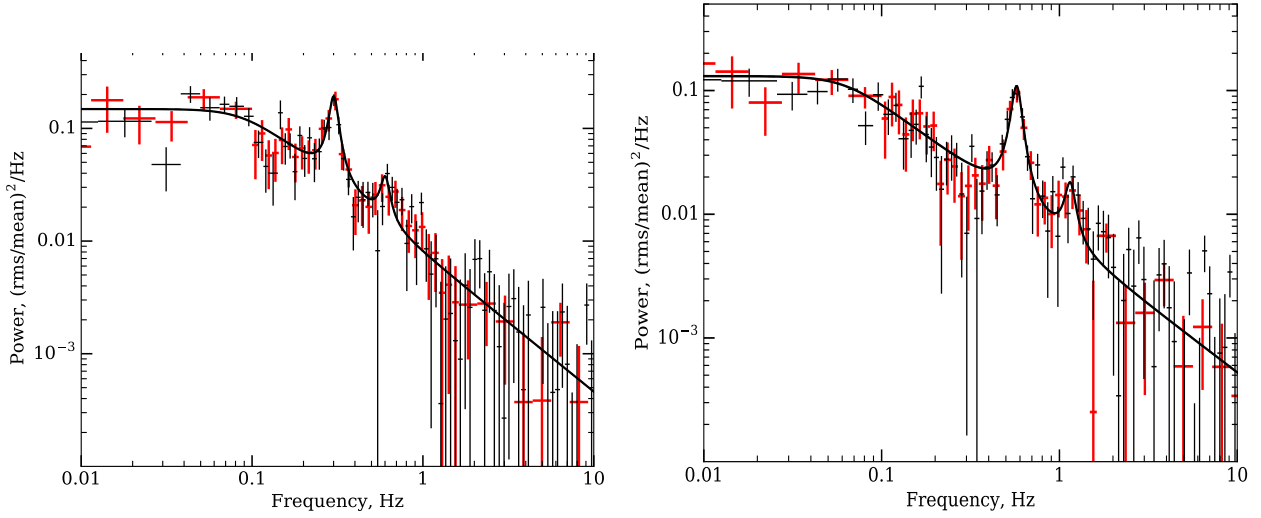
Figure 6. On the left panel power spectrum and cospectrum obtained in the soft band at the beginning of *NuSTAR* observation. On the right column same spectra obtained at the end of the observation. Red crosses correspond to the power spectrum with Poisson noise component subtracted, and black crosses correspond to cospectrum. Black line represents best model for the power spectrum without Poisson noise component.

Table 2. Evolution of the Fourier and energy spectrum properties through the *NuSTAR* observation in the 3–5 keV energy band.

Interval	T_{start}, MJD	Expo, s	f_{br}, $\times 10^{-2}$, Hz	f_{QPO}, Hz	Q_m, $\times 10^{-2}$	A_m, (rms/mean) %	A_o, (rms/mean) %	rms, %	Γ	E_{cut}, keV
I	56742.68	3386	$9.0^{+2.5}_{-2.5}$	0.30 ± 0.01	$7.2^{+2.5}_{-1.8}$	$7.4^{+1.1}_{-1.3}$	$3.9^{+1.1}_{-1.2}$	27 ± 3	1.46 ± 0.01	29.9 ± 0.4
II	56742.75	3388	$8.8^{+2.6}_{-2.3}$	0.31 ± 0.01	$8.5^{+2.6}_{-2.2}$	7.6 ± 1.2	$3.3^{+1.1}_{-1.2}$	24^{+3}_{-2}	1.46 ± 0.01	30.7 ± 0.4
III	56742.81	3392	$9.1^{+3.2}_{-2.2}$	0.34 ± 0.01	$8.7^{+3.3}_{-2.2}$	7.2 ± 1.2	$3.9^{+1.0}_{-1.2}$	26 ± 3	1.46 ± 0.01	29.7 ± 0.4
IV	56742.88	3389	$8.3^{+2.5}_{-2.1}$	0.35 ± 0.01	$8.6^{+2.4}_{-1.9}$	$7.3^{+1.1}_{-1.2}$	$4.2^{+1.1}_{-1.2}$	27^{+4}_{-3}	1.47 ± 0.01	$29.5^{+0.4}_{-0.3}$
V	56742.95	3389	$7.2^{+2.0}_{-1.9}$	0.39 ± 0.01	$8.6^{+2.7}_{-2.1}$	$7.1^{+1.0}_{-1.1}$	$4.4^{+1.2}_{-1.3}$	27^{+4}_{-3}	1.47 ± 0.01	28.6 ± 0.3
VI	56743.02	3136	$7.2^{+2.1}_{-2.0}$	0.41 ± 0.01	$7.1^{+2.0}_{-1.8}$	7.0 ± 1.1	$4.8^{+1.1}_{-1.2}$	27^{+4}_{-3}	1.47 ± 0.01	28.1 ± 0.3
VII	56743.09	2771	$8.4^{+2.5}_{-2.2}$	0.42 ± 0.02	$13.0^{+4.0}_{-3.0}$	$7.3^{+1.2}_{-1.2}$	$4.1^{+1.4}_{-1.2}$	25^{+4}_{-3}	1.50 ± 0.01	28.7 ± 0.4
VIII	56743.15	3387	$6.0^{+1.8}_{-1.7}$	0.46 ± 0.01	$7.2^{+2.5}_{-1.9}$	$6.6^{+1.1}_{-1.1}$	$3.8^{+1.1}_{-1.3}$	30^{+6}_{-5}	1.51 ± 0.01	29.3 ± 0.4
IX	56743.22	3392	$13.0^{+3.0}_{-3.0}$	0.49 ± 0.02	$15.0^{+4.0}_{-3.0}$	$9.8^{+0.9}_{-1.1}$	$6.6^{+1.0}_{-1.2}$	21 ± 1	1.50 ± 0.01	28.1 ± 0.3
X	56743.29	3390	$7.9^{+2.4}_{-2.5}$	0.54 ± 0.01	$7.8^{+2.1}_{-1.9}$	$7.9^{+1.1}_{-1.0}$	$5.3^{+1.2}_{-1.0}$	26^{+5}_{-3}	1.50 ± 0.01	27.2 ± 0.3
XI	56743.35	3382	$6.3^{+2.3}_{-1.9}$	0.57 ± 0.01	$7.8^{+2.0}_{-1.7}$	8.3 ± 1.0	$4.1^{+1.1}_{-1.4}$	26^{+5}_{-3}	1.53 ± 0.01	28.7 ± 0.3
XII	56743.42	3386	$7.1^{+2.4}_{-2.2}$	0.63 ± 0.01	$8.8^{+2.7}_{-1.7}$	$8.9^{+1.0}_{-1.1}$	$5.1^{+1.2}_{-1.3}$	26^{+6}_{-3}	1.53 ± 0.01	27.5 ± 0.3
XIII	56743.49	3391	$6.8^{+2.2}_{-2.1}$	0.67 ± 0.01	$6.5^{+2.0}_{-1.4}$	$8.8^{+1.0}_{-0.9}$	$4.4^{+1.1}_{-1.2}$	27^{+6}_{-4}	1.53 ± 0.01	26.2 ± 0.3

the following expression:

$$C(f) = \frac{|<H(f)^*S(f)>|^2 - n^2}{<|H(f)|^2><|S(f)|^2>} \qquad (2)$$

where $H(f)$ and $S(f)$ are Fourier function (corrected for the Poisson noise components) of the time series in hard and soft bands correspondingly, n^2 - product of the power in uncorrelated components, connected with counting statistic, divided by the number of used series. Coherence should be computed for the number of independent time intervals, therefore we separated each of the available uninterrupted time series on several shorter parts, 82 s long each.

Coherence is very similar to cospectrum, but instead of tracking signals with zero phase shifts, it's track all signals with arbitrary conserved phase shift - i.e. Fourier harmonics of the signals may delay each other but be coherent (which means that Fourier functions $H(f)$ and $S(f)$ are related by linear transformation (Vaughan and Nowak 1997)). It should

be noted that from this definition of coherence it follows that coherent signals (with unity coherence along all Fourier frequencies) may not be similar in time domain.

Different models of the XBs variability generation suggest that the signal in two energy bands can be partially independent, while the shape of the power spectra is conserved. It appears that in many sources coherence between soft and hard X-ray bands is close to unity (Nowak et al. 1999; Wijnands and van der Klis 1999b), however there also was indications on complex picture of the coherence in particular state of some systems (Ji et al. 2003), or drop in coherence between particular energy bands (e.g. in GX 339–4 Vaughan and Nowak 1997). See also discussion in the (Vaughan and Nowak 1997) for the theoretical prediction on the coherence for different models.

Following (Vaughan and Nowak 1997), we estimated correlation of GRS 1739–278 light-curves obtained in differ-
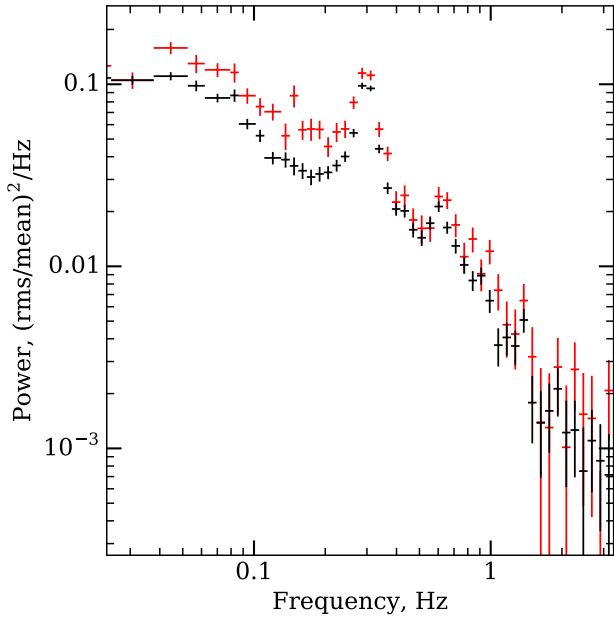
Figure 7. Cross-spectrum of the observations, obtained by scaling frequency to conserve QPO position. Black crosses obtained from the all data sets, while red crosses are from sets I, II, IV, and V, in which QPO subharmonics was most prominent.
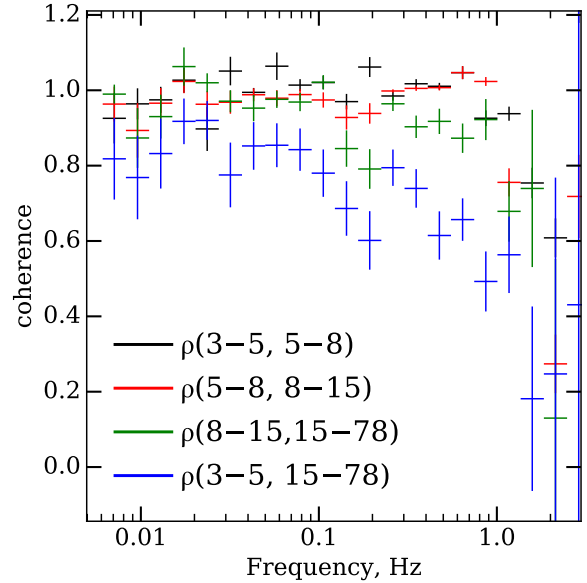

Figure 8. Coherence between different energy bands: red crosses between 3–5 and 5–8 keV, green crosses between 5–8 and 8–15 keV, blue crosses between 8–15 and 15–78 keV, black crosses between 3–5 and 15–78 keV.

ent soft and hard energy bands. Since for the timing analysis we use *NuSTAR* data, covering 3–79 keV energy bands, we adopted following energy bands for our analysis: 3–5 keV, 5–8 keV, 8–15 keV and 15–78 keV. This partition of the *NuSTAR* energy band pursues the following idea: despite the energy spectrum of GRS 1739–278 can be described with the two major components - powerlaw continuum and fluorescent Fe Kα line, we can expect that each of chosen energy bands is dominated by the processes with slightly different origin. The Fe Kα line has equivalent width approximately 0.2 keV, therefore producing only 5% of the flux in the 5–8 keV and must be anchored to some source of the hard photons depending on the system geometry, e.g. in the lamp post geometry it should be coherent with the hard power-law emission. In the 8–15 keV energy band we expecting the hard powerlaw corona emission to be the dominant, while in the 15–78 keV Compton hump may be presented.

Since the *NuSTAR* detectors have complex dead-time depending on energy (see Bachetti et al. 2015, for a details on how this affects power spectra), coherence computed from one detector is subject to the dead-time crosstalk effects (which should make random processes more coherent). In order to eliminate this effects, following the recipe suggested in Bachetti et al. (2015) for cospectrum estimation, for the numerator in Eq. 2 we used cross-products of the light-curves Fourier functions obtained from the different modules - e.g. correlations of the light-curve obtained in the soft band on the FPMA module with the light-curve in the hard band obtained in the FPMB and vice versa. In the obtained cross-product dead-time cross-talk effects is significantly dumped. We also use cospectrum obtained for each energy band as the estimation for the denominator in the Eq. 2. The n^2 component was computed as it is suggested in (Vaughan

and Nowak 1997), however for the Poisson noise components power estimation we used mean value of the power spectra in the 5–20 Hz range, assuming that Poisson noise dominating intrinsic source variability and constant along frequencies.

Wijnands and van der Klis (1999a) shown that primary features of the Power spectrum of the XBs in low-hard state are evolving simultaneously, i.e. flat top broad band noise break frequency and QPO centroid frequency are connected with the relation $f_b \approx 0.3 f_{qpo}$. Therefore, in order to improve significance of the coherence measurements, and bearing in mind aforementioned property of the power spectrum, we stacked all 13 separate parts of the observation, scaling their frequencies to preserve QPO position. We also assumed that the coherence is preserved along the observation.

On Figure 8 presented measured coherence between hard and soft bands on the frequencies up to ~ 1 Hz. We found that coherence in the neighboring energy hands is close to unity, with mean values in 0.01–1 Hz frequency band being 1.0 ± 0.05, however we found that for the 3–5 and 15–78 keV energy bands the coherence is significantly lower, see Fig. 8. It is on the nearly constant level of 0.85 in the 0.01–0.3 Hz frequency band and drops down above this frequency. SInce the loss of the coherence is also observed above 0.3–1.0 Hz frequency for other energy bands, this effect may be connected not with the intrinsic properties of the source, but with the bead-time cross-talk effects which we did not specially consider, except for using light-curves from the different *NuSTAR* modules for cross-products.

5.3 Phase lags

Following (Vaughan and Nowak 1997) we estimated phase lag as an angle of mean product of the light

curves Fourier harmonics from one energy bands to the conjugated Fourier harmonics of second energy band. We can imagine that each light curve from a sample consist of a stochastic noise and coherent signal $S \exp -i(\alpha(s,h) + U_{h=s}[-\pi, \pi]) + N \exp -iU[-\pi, \pi]$, where S and N amplitudes of coherent signals and noise correspondingly and U - uniform distribution, $U_{h=s}$ stands for random phase shift equal for the signals in hard and soft bands, and $\alpha(s,h)$ - phase shift between soft and hard bands. Therefore the product of the Fourier signals from two bands is $S_s S_h \exp -i\alpha(s,h) + (S_s * N_h + S_h * N_s + N_h * N_s) \exp -iU[-\pi,$ (**?**) pointer out that the product of two normally distributed values has probability density function (PDF) of the form of special Bessel function of second kind with zero order. It follows that noise components in the Brackets is a sum of three random numbers with PDF = K_0, with not equal moments, phase of the coherent part is either well defined or distributed around some particular phase shift. We can now determine the "phase axis" as the axis along the mean complex value of the Sample. Distribution of the points relative to the "phase axis" obviously should be symmetrical, and along it should be assymetric and shifted towards the mean complex value of the sample. If we now rotate all the obtained complex Fourier harmonics in our sample along this axis $\frac{<P_{hs}^*>P_{hs}}{|<P_{hs}>|}$, real part of each value is the projection on the "phase axis" and imaginary part is projection on the perpendicular axis. We found that the distribution of the projected on the "phase axis" values is closely resembles assymetric Laplace distribution and the distribution of the points projected on the perpendicular axis resembles symmetric Laplace distribution. Bearing this in mind we estimate mean value for each of the four distributions (positive real, negative real, positive imaginary and negative imaginary) and assess variances of this distribution. Since we accepted that each of these distribution has a PDF close to exponential we take their variance as a variance of χ_2^{2N} distribution, where N - is a number of entities in the each sample. After that we accept the error on the phase to be equal π if the mean of positive real sample is less than the square root of the sum of the positive and negative real samples variances, otherwise we take it to be equal

$$\Delta\phi = atan\left(\frac{\sqrt{v_{i-}^2 + v_{i+}^2}}{m_{r+} - m_{r-} - \sqrt{v_{r+}^2 + v_{r-}^2}}\right) \quad (3)$$

Most of the models of the accretion flow which describe variability and energy spectra formation, suggest the time lag between the signals in different energy bands. For example in some models of the energy spectra formation, time lag is naturally arise due to the geometry of the corona and properties of the inverse Comptonization process (see, e.g. **?**). Phase lag is also suggested from the propagating fluctuations model - hard photons are emitted from the inner parts of the accretion flow from the perturbations, which initially were born in the outer parts of the disk were produce soft emission.

(**?**) have found, that the phase lag of XBs, probably depends on the system inclination angle, it also definitely contain information about the characteristic times of the system, and therefore can be proxy to the compact object mass ().
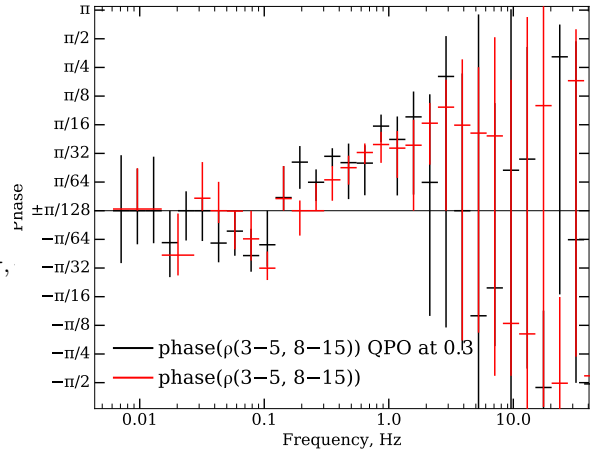
Figure 9. Phase lag between the hard (3–5 keV) and soft (8–15) energy bands in GRS 1739–278

Phase lags can be estimated as a product of the mean phase of the set of Fourier spectra and the corresponding frequency:

$$\tau = \frac{\phi(f)}{2\pi f} \quad (4)$$

$$\phi(f) = < arccos\left(\frac{re(< F_h^*(f)F_s(f) >)}{|F_h^*(f)F_s(f)|}\right) > \quad (5)$$

here, $F_h(f)$ and $F_s(f)$ are Fourier functions of the lightcurves in the hard and soft bands, $\phi(f)$ is the phase lag.

Phase lag between 3–5 and 8–15 keV energy bands for frequencies from 10^{-2} Hz to 10 Hz is presented in Figure 9. To measure phase lags we use two approaches, first we estimated with the frequency scaling, as it was described in the previous part, second we estimated phase lag on the raw frequency suggesting that it do not changing with time. Surprisingly, both pictures appears to be very similar, it should be noted that some observations suggested that the phase lag changes with the QPO frequency ()

It appears that the phase lags is generally positive (hard lag) on the frequencies 0.1–2 Hz, and also can be described with the shifted power law $\propto (f - f_0)^{0.3}$. Above 2 Hz significance of the phase lags estimation drops due to the Poisson noise. In the range 0.03–0.1 Hz there is a week indication on the negative phase lag with the mean value $\approx 0.02\pi$, which corresponds to the time ≈ 0.1 s.

5.4 *Swift-XRT* observations

We performed search for LF QPOs in first dosen of *Swift-XRT* observations of the GRS 1739–278 . QPO is clearly detected in observations 3 to 9, with frequency varying from 0.4 Hz (during simultaneous observation with *NuSTAR*, see Fig. 2) up to 5 Hz (see Tab. 3). Due to typically short exposures of *Swift-XRT* snapshots (about 1 ks) it is hard to classify QPOs as belonging to type C or B, because low-frequency part of power spectra lacks statistics, yet, except for the first detection (segment 03) power spectra were red-noise like, without strong low-frequency components. We

Table 3. QPOs detected in *Swift-XRT* observations

Segment	f_{QPO}, Hz	rms, %	Type
03	0.4	14%	C
04	2.2	11%	B
05	1.7	13%	B
06	5.0	6%	B
07	2.5	10%	B
08	5.1	7%	B
09	2.2	11%	B

calculated *rms* for each detected QPO - most of them is higher than 10%, which is not typical for type C QPO (Casella et al. 2005).

6 DISCUSSION

We had studied the spectra-timing evolution of the GRS 1739–278 during its hard-intermediate state. The frequency of type-C LF QPO show clear correlation with properties of continuum emission. As the QPO frequency increases form 0.3 to 0.7 Hz spectrum became softer: the power law index grows from 1.46 to 1.53 and cut-off energy decreases from 30 to 26 keV. Overall flux increases, too. This behaviour was first observed in a number of systems by Di Matteo and Psaltis (1999) and now it is studied in greater details in many systems (see e.g. Vignarca et al. 2003b; Stiele et al. 2013; Seifina et al. 2014; Fürst et al. 2016, and many more). Although the quality of a data prevented us from measuring a movement of the inner disk boundary, from the total broadband spectrum we found that an accretion disk is truncated at radius smaller than 8 GM/c^2 (90% confidence limit) which is in agreement with an estimates by Miller et al. (2015). This allowed us to check if this combination of inner radius and frequency is consistent with the popular model of QPO generation such as Lense-Thirring precession (Ingram et al. 2009a). Following the calculations of Ingram and Motta (2014) we caluclated nodal frequencies (which is though to correspond to QPO fundamental frequency) versus inner radius for two values of black hole mass ($10M_\odot$ and $30M_\odot$) and two values of spin - $a = 0.1$ and $a = 0.998$ (maximally rotating). As it can be seen from Fig. 10 observations are incompatible with expected values for $10M_\odot$ black hole and barely agrees with slowly rotating massive black hole. This results, along with measurements by Fürst et al. (2016), indicate that there are some tensions between predictions of RPM and truncation radii inferred from spectral fitting.

We carried out extensive study of timing properties of the GRS 1739–278. Along with broadband noise and fundamental QPO first overtone of QPO is clearly seen. During several intervals from first half of the observation subharmonic was seen too. Break frequency of broadband noise is correlated with QPO frequency following the WK relation (Wijnands and van der Klis 1999a). In all 13 intervals first QPO overtone is more prominent in soft band (3–5 keV), with relation of its amplitude to that of fundamental QPO being 0.4(1) in 3–5 keV band versus 0.2(1) in 10–78 keV. We also measure velocity of QPO drift and found it
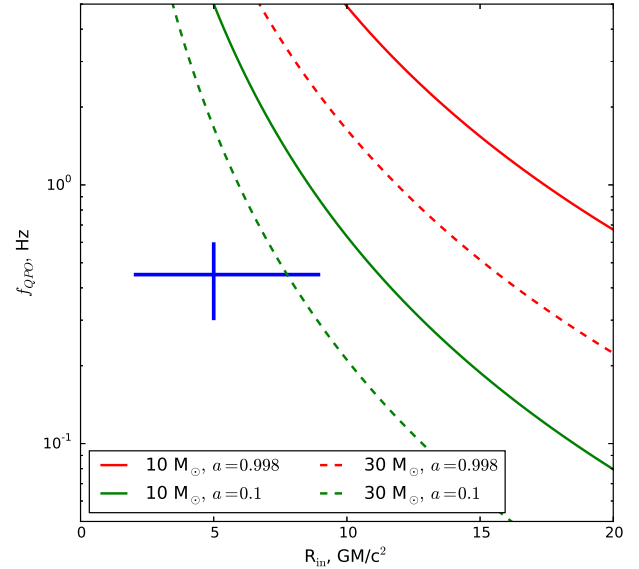

Figure 10. Expected QPO frequency for a black hole of a given mass and spin versus inner disk radius from Ingram and Motta (2014). Blue point correspond to measured inner disk radius and range of observed QPO frequencies.

to be 7.0×10^{-6} Hz s^{-1}. We searched for similar QPO in *Swift-XRT* observations of the GRS 1739–278 performed after *NuSTAR* exposure and found that all other detected QPOs are probably of type B, thus indicating that the type-C QPO reach saturation on frequencies below few Hz. Coherence measured between adjacent energy ranges in 0.01-1 Hz was found to be nearly unity, while for distant energy coherence turned out to be lower. Phase lag found to be ....

REFERENCES

Arévalo, P. and Uttley, P.: 2006, *MNRAS* **367**, 801
Arnaud, K. A.: 1996, in G. H. Jacoby and J. Barnes (eds.), *Astronomical Data Analysis Software and Systems V*, Vol. 101 of *Astronomical Society of the Pacific Conference Series*, p. 17
Bachetti, M., Harrison, F. A., Cook, R., Tomsick, J., Schmid, C., Grefenstette, B. W., Barret, D., Boggs, S. E., Christensen, F. E., Craig, W. W., Fabian, A. C., Fürst, F., Gandhi, P., Hailey, C. J., Kara, E., Maccarone, T. J., Miller, J. M., Pottschmidt, K., Stern, D., Uttley, P., Walton, D. J., Wilms, J., and Zhang, W. W.: 2015, *ApJ* **800**, 109
Belloni, T. and Hasinger, G.: 1990, *A&A* **227**, L33
Belloni, T. M.: 2010, in T. Belloni (ed.), *Lecture Notes in Physics, Berlin Springer Verlag*, Vol. 794 of *Lecture Notes in Physics, Berlin Springer Verlag*, p. 53
Borozdin, K. N., Revnivtsev, M. G., Trudolyubov, S. P., Aleksandrovich, N. L., Sunyaev, R. A., and Skinner, G. K.: 1998, *Astronomy Letters* **24**, 435
Borozdin, K. N. and Trudolyubov, S. P.: 2000, *ApJ* **533**, L131
Cabanac, C., Henri, G., Petrucci, P.-O., Malzac, J., Ferreira, J., and Belloni, T. M.: 2010, *MNRAS* **404**, 738
Casella, P., Belloni, T., and Stella, L.: 2005, *ApJ* **629**, 403
Churazov, E., Gilfanov, M., and Revnivtsev, M.: 2001, *MNRAS* **321**, 759

Dauser, T., García, J., Parker, M. L., Fabian, A. C., and Wilms, J.: 2014, *MNRAS* **444**, L100

Dauser, T., García, J., Walton, D. J., Eikmann, W., Kallman, T., McClintock, J., and Wilms, J.: 2016, *A&A* **590**, A76

Di Matteo, T. and Psaltis, D.: 1999, *ApJ* **526**, L101

Eardley, D. M., Lightman, A. P., and Shapiro, S. L.: 1975, *ApJ* **199**, L153

Evans, P. A., Beardmore, A. P., Page, K. L., Osborne, J. P., O'Brien, P. T., Willingale, R., Starling, R. L. C., Burrows, D. N., Godet, O., Vetere, L., Racusin, J., Goad, M. R., Wiersema, K., Angelini, L., Capalbi, M., Chincarini, G., Gehrels, N., Kennea, J. A., Margutti, R., Morris, D. C., Mountford, C. J., Pagani, C., Perri, M., Romano, P., and Tanvir, N.: 2009, *MNRAS* **397**, 1177

Filippova, E., Kuulkers, E., Skådt, N. M., Alfonso-Garzon, J., Beckmann, V., Bird, A. J., Brandt, S., Chenevez, J., Del Santo, M., Domingo, A., Ebisawa, K., Jonker, P. G., Kretschmar, P., Markwardt, C. B., Oosterbroek, T., Paizis, A., Pottschmidt, K., Sanchez-Fernandez, C., Wijnands, R., Bozzo, E., and Ferrigno, C.: 2014, *The Astronomer's Telegram* 5991

Fuerst, F., Tomsick, J. A., Yamaoka, K., Dauser, T., Miller, J. M., Clavel, M., Corbel, S., Fabian, A. C., Garcia, J., Harrison, F. A., Loh, A., Kaaret, P., Kalemci, E., Migliari, S., Miller-Jones, J. C. A., Pottschmidt, K., Rahoui, F., Rodriguez, J., Stern, D., Stuhlinger, M., Walton, D. J., and Wilms, J.: 2016, *ArXiv e-prints*

Fürst, F., Grinberg, V., Tomsick, J. A., Bachetti, M., Boggs, S. E., Brightman, M., Christensen, F. E., Craig, W. W., Gandhi, P., Grefenstette, B., Hailey, C. J., Harrison, F. A., Madsen, K. K., Parker, M. L., Pottschmidt, K., Stern, D., Walton, D. J., Wilms, J., and Zhang, W. W.: 2016, *ApJ* **828**, 34

García, J., Dauser, T., Reynolds, C. S., Kallman, T. R., McClintock, J. E., Wilms, J., and Eikmann, W.: 2013, *ApJ* **768**, 146

Grebenev, S. A., Sunyaev, R. A., and Pavlinsky, M. N.: 1997, *Advances in Space Research* **19**, 15

Greiner, J., Dennerl, K., and Predehl, P.: 1996, *A&A* **314**, L21

Harrison, F. A., Craig, W. W., Christensen, F. E., Hailey, C. J., Zhang, W. W., Boggs, S. E., Stern, D., Cook, W. R., Forster, K., Giommi, P., Grefenstette, B. W., Kim, Y., Kitaguchi, T., Koglin, J. E., Madsen, K. K., Mao, P. H., Miyasaka, H., Mori, K., Perri, M., Pivovaroff, M. J., Puccetti, S., Rana, V. R., Westergaard, N. J., Willis, J., Zoglauer, A., An, H., Bachetti, M., Barrière, N. M., Bellm, E. C., Bhalerao, V., Brejnholt, N. F., Fuerst, F., Liebe, C. C., Markwardt, C. B., Nynka, M., Vogel, J. K., Walton, D. J., Wik, D. R., Alexander, D. M., Cominsky, L. R., Hornschemeier, A. E., Hornstrup, A., Kaspi, V. M., Madejski, G. M., Matt, G., Molendi, S., Smith, D. M., Tomsick, J. A., Ajello, M., Ballantyne, D. R., Baloković, M., Barret, D., Bauer, F. E., Blandford, R. D., Brandt, W. N., Brenneman, L. W., Chiang, J., Chakrabarty, D., Chenevez, J., Comastri, A., Dufour, F., Elvis, M., Fabian, A. C., Farrah, D., Fryer, C. L., Gotthelf, E. V., Grindlay, J. E., Helfand, D. J., Krivonos, R., Meier, D. L., Miller, J. M., Natalucci, L., Ogle, P., Ofek, E. O., Ptak, A., Reynolds, S. P., Rigby, J. R., Tagliaferri, G., Thorsett, S. E., Treister, E., and Urry, C. M.: 2013, *ApJ* **770**, 103

Heil, L. M., Uttley, P., and Klein-Wolt, M.: 2015, *MNRAS* **448**, 3339

Hjellming, R. M., Rupen, M. P., Marti, J., Mirabel, F., and Rodriguez, L. F.: 1996, *IAU Circ.* 6383

Homan, J. and Belloni, T.: 2005a, *Ap&SS* **300**, 107

Homan, J. and Belloni, T.: 2005b, *Ap&SS* **300**, 107

Ingram, A., Done, C., and Fragile, P. C.: 2009a, *MNRAS* **397**, L101

Ingram, A., Done, C., and Fragile, P. C.: 2009b, *MNRAS* **397**, L101

Ingram, A. and Motta, S.: 2014, *MNRAS* **444**, 2065

Ingram, A. and van der Klis, M.: 2013, *MNRAS* **434**, 1476

Ingram, A. and van der Klis, M.: 2015, *MNRAS* **446**, 3516

Ingram, A., van der Klis, M., Middleton, M., Done, C., Altamirano, D., Heil, L., Uttley, P., and Axelsson, M.: 2016, *MNRAS* **461**, 1967

Ji, J. F., Zhang, S. N., Qu, J. L., and Li, T. P.: 2003, *ApJ* **584**, L23

Krimm, H. A., Barthelmy, S. D., Baumgartner, W., Cummings, J., Gehrels, N., Lien, A. Y., Markwardt, C. B., Palmer, D., Sakamoto, T., Stamatikos, M., and Ukwatta, T.: 2014, *The Astronomer's Telegram* 5986

Krimm, H. A., Holland, S. T., Corbet, R. H. D., Pearlman, A. B., Romano, P., Kennea, J. A., Bloom, J. S., Barthelmy, S. D., Baumgartner, W. H., Cummings, J. R., Gehrels, N., Lien, A. Y., Markwardt, C. B., Palmer, D. M., Sakamoto, T., Stamatikos, M., and Ukwatta, T. N.: 2013, *ApJS* **209**, 14

Lyubarskii, Y. E.: 1997, *MNRAS* **292**, 679

Marti, J., Mirabel, I. F., Duc, P.-A., and Rodriguez, L. F.: 1997, *A&A* **323**, 158

Matsuoka, M., Kawasaki, K., Ueno, S., Tomida, H., Kohama, M., Suzuki, M., Adachi, Y., Ishikawa, M., Mihara, T., Sugizaki, M., Isobe, N., Nakagawa, Y., Tsunemi, H., Miyata, E., Kawai, N., Kataoka, J., Morii, M., Yoshida, A., Negoro, H., Nakajima, M., Ueda, Y., Chujo, H., Yamaoka, K., Yamazaki, O., Nakahira, S., You, T., Ishiwata, R., Miyoshi, S., Eguchi, S., Hiroi, K., Katayama, H., and Ebisawa, K.: 2009, *PASJ* **61**, 999

Mereminskiy, I., Krivonos, R., Grebenev, S., Filippova, E., and Sunyaev, R.: 2016, *The Astronomer's Telegram* 9517

Miller, J. M., Homan, J., and Miniutti, G.: 2006a, *ApJ* **652**, L113

Miller, J. M., Homan, J., Steeghs, D., Rupen, M., Hunstead, R. W., Wijnands, R., Charles, P. A., and Fabian, A. C.: 2006b, *ApJ* **653**, 525

Miller, J. M., Tomsick, J. A., Bachetti, M., Wilkins, D., Boggs, S. E., Christensen, F. E., Craig, W. W., Fabian, A. C., Grefenstette, B. W., Hailey, C. J., Harrison, F. A., Kara, E., King, A. L., Stern, D. K., and Zhang, W. W.: 2015, *ApJ* **799**, L6

Molteni, D., Sponholz, H., and Chakrabarti, S. K.: 1996, *ApJ* **457**, 805

Narayan, R. and Yi, I.: 1995, *ApJ* **452**, 710

Nowak, M. A., Wilms, J., and Dove, J. B.: 1999, *ApJ* **517**, 355

Parker, M. L., Tomsick, J. A., Miller, J. M., Yamaoka, K., Lohfink, A., Nowak, M., Fabian, A. C., Alston, W. N., Boggs, S. E., Christensen, F. E., Craig, W. W., Fürst, F., Gandhi, P., Grefenstette, B. W., Grinberg, V., Hailey, C. J., Harrison, F. A., Kara, E., King, A. L., Stern, D., Walton, D. J., Wilms, J., and Zhang, W. W.: 2015, *ApJ* **808**, 9

Paul, J., Bouchet, L., Churazov, E., and Sunyaev, R.: 1996, *IAU Circ.* 6348

Paul, J., Mandrou, P., Ballet, J., Cantin, M., Chabaud, J., Cordier, B., Ehanno, M., Goldwurm, A., Lambert, A., Lande, J., et al.: 1991, *Advances in Space Research* **11(8)**, 289

Pottschmidt, K., Wilms, J., Nowak, M. A., Pooley, G. G., Gleissner, T., Heindl, W. A., Smith, D. M., Remillard, R., and Staubert, R.: 2003, *A&A* **407**, 1039

Remillard, R. A. and McClintock, J. E.: 2006, *ARA&A* **44**, 49

Ross, R. R. and Fabian, A. C.: 2005, *MNRAS* **358**, 211

Schnittman, J. D., Homan, J., and Miller, J. M.: 2006, *ApJ* **642**, 420

Seifina, E., Titarchuk, L., and Shaposhnikov, N.: 2014, *ApJ* **789**, 57

Shakura, N. I. and Sunyaev, R. A.: 1973, *A&A* **24**, 337

Shapiro, S. L., Lightman, A. P., and Eardley, D. M.: 1976, *ApJ* **204**, 187

Stella, L. and Vietri, M.: 1998a, *ApJ* **492**, L59

Stella, L. and Vietri, M.: 1998b, *ApJ* **492**, L59

Stiele, H., Belloni, T. M., Kalemci, E., and Motta, S.: 2013, *MN-*

RAS **429**, 2655

Tagger, M. and Pellat, R.: 1999, *A&A* **349**, 1003

Tanaka, Y. and Shibazaki, N.: 1996, *ARA&A* **34**, 607

Terrell, Jr., N. J.: 1972, *ApJ* **174**, L35

García, J., Dauser, T., Lohfink, A., Kallman, T. R., Steiner, J. F., McClintock, J. E., Brenneman, L., Wilms, J., Eikmann, W., Reynolds, C. S., and Tombesi, F.: 2014, *ApJ* **782**, 76

Vaughan, B. A. and Nowak, M. A.: 1997, *ApJ* **474**, L43

Verner, D. A., Ferland, G. J., Korista, K. T., and Yakovlev, D. G.: 1996, *ApJ* **465**, 487

Vignarca, F., Migliari, S., Belloni, T., Psaltis, D., and van der Klis, M.: 2003a, *A&A* **397**, 729

Vignarca, F., Migliari, S., Belloni, T., Psaltis, D., and van der Klis, M.: 2003b, *A&A* **397**, 729

Wijnands, R. and van der Klis, M.: 1999a, *ApJ* **514**, 939

Wijnands, R. and van der Klis, M.: 1999b, *ApJ* **514**, 939

Wilms, J., Allen, A., and McCray, R.: 2000, *ApJ* **542**, 914

Yan, Z. and Yu, W.: 2017, *Monthly Notices of the Royal Astronomical Society* **470(4)**, 4298

This paper has been typeset from a TeX/LaTeX file prepared by the author.